The landscape of genetic alterations of UVB-induced skin tumors in DNA repair-deficient mice

Yoshioka, Ai ; Nakaoka, Hirofumi ; Fukumoto, Takeshi ; Inoue, Ituro ; Nishigori, Chikako ; Kunisada, Makoto

(Citation)
Experimental Dermatology,31(10):1607-1617

(Issue Date)
2022-10-01

(Resource Type)
journal article

(Version)
Accepted Manuscript

The landscape of genetic alterations of UVB-induced skin tumors in DNA repair-deficient mice

Ai Yoshioka[1], Hirofumi Nakaoka[2,3], Takeshi Fukumoto[1], Ituro Inoue[3], Chikako Nishigori[4],

*Makoto Kunisada.[1]

[1]Division of Dermatology, Department of Internal Related, Graduate School of Medicine, Kobe University, Kobe, Japan.
[2]Department of Cancer Genome Research, Sasaki Institute, Tokyo, Japan
[3]Human Genetics Laboratory, National Institute of Genetics, Mishima, Japan
[4]Division of Research on Intractable Dermatological Disease, Department of iPS cell Applications, Kobe University Graduate School of Medicine, Kobe, Japan

*Corresponding author:

Makoto Kunisada, Division of Dermatology, Department of Internal Related, Graduate School of Medicine, Kobe University, Kobe 650-0017, Japan.

Phone: 81-78-382-6134; Fax: 81-78-382-6149; E-mail: kunisada@med.kobe-u.ac.jp

Funding information

This work was partially supported by a Grant-in-Aid 19k08749 from the Ministry of Education, Culture, Sports, Science, and Technology of Japan (MEXT) (MK) and Challenging Exploratory Research Projects for the Future grant from the Research

Organization of Information and Systems (ROIS) (HN). This research was supported by AMED under Grant Numbers JP20ek0109450h0001 (CN, MK) and JP20ek0109488 (CN).

Abstract

Non-melanoma skin cancer (NMSC) is mainly caused by ultraviolet (UV)-induced somatic mutations and is characterized by UV signature modifications. Xeroderma pigmentosum group A (*Xpa*) knockout mice exhibit extreme UV-induced photo-skin carcinogenesis, along with a photosensitive phenotype. We performed whole-exome sequencing (WES) of squamous cell carcinoma (SCC) samples after repetitive ultraviolet B (UVB) exposure to investigate the differences in the landscape of somatic mutations between *Xpa* knockout and wild-type mice. Although the tumors that developed in mice harbored UV signature mutations in a similar set of cancer-related genes, the pattern of transcriptional strand asymmetry was largely different; UV signature mutations in *Xpa* knockout and wild-type mice preferentially occurred in transcribed and non-transcribed strands, respectively, reflecting a deficiency in transcription-coupled nucleotide excision repair in *Xpa* knockout mice. Serial time point analyses of WES for a tumor induced by only a single UVB exposure showed pathogenic mutations in *Kras*, *Fat1*, and *Kmt2c*, which may be driver genes for the initiation and promotion of SCC in *Xpa* knockout mice. Furthermore, the inhibitory effects on tumor production in *Xpa* knockout mice by the anti-inflammatory CXCL1 monoclonal antibody affected the pattern of somatic mutations, wherein the

transcriptional strand asymmetry was attenuated and the activated signal transduction was shifted from the RAS/RAF/MAPK to the PIK3CA pathway.

Keywords: skin carcinogenesis, UVB, *Xpa* deficient mice, whole genome sequencing, transcribed strand

1 INTRODUCTION

Non-melanoma skin cancer (NMSC) and melanoma are caused mostly by somatic mutations stemming from ultraviolet (UV)-induced cyclobutane pyrimidine dimer (CPD) formation and pyrimidine (6-4) photoproducts (6-4 PPs), which are UV-specific DNA damage and are pivotal events in UV-induced skin cancer [1,2]. UV-induced human skin carcinogenesis is considered a multi-stepwise mechanism, that is, initiation, promotion, and progression, similar to that of chemical carcinogen-induced mouse papilloma and cancers [3,4]. The tumor suppressor gene (TSG) *TRP53* and oncogene *RAS* are well known as key genes involved in UV-induced skin carcinogenesis [5-7]. Recently, somatic mutations in *NOTCH1* (*Notch1*) and *NOTCH2* (*Notch2*) have been frequently observed in cutaneous squamous cell carcinoma (SCC) in humans and mice as a TSG [8,9], and they occur even in normal skin, suggesting that alterations in these genes are driver mutations in the very early stages of the development of human NMSC [10].

UV-induced CPDs and 6-4 PPs as dipyrimidine photoproducts, essentially deaminated cytosine-containing dimeric lesions, are highly mutation-prone DNA lesions if not repaired by the nucleotide excision repair (NER) system. One of the most distinctive NER-defective human phenotypes is xeroderma pigmentosum complementation group A (XP-A), which is a rare autosomal recessive hereditary disease characterized by more

than 10,000-fold and 2,000-fold increased risk of NMSC and melanoma, respectively [11], and) Model mice (*Xpa* knockout mice) have been widely utilized for studies on the mechanism of NMSC development [12]. Another important UV-induced DNA damage involved in skin cancer development is reactive oxygen species (ROS)-induced DNA modification. 7,8-dihydro-8-oxoguaanine (8-oxoG) is a major DNA damage induced by ROS and can cause G:C>T:A transversion [13]. 8-oxoG of DNA in the epidermis is also induced by UV irradiation. Deficiencies in the repair enzyme for 8-oxoG can lead to a more carcinogenic phenotype in mice [14,15]. Skin carcinogenesis is also pronounced in *Xpa* knockout mice, where presumably more ROS retention is observed after exposure to UVB (wavelength:280–315 nm) exposure [16]. However, the landscape of somatic mutations that drive such extreme phenotypes has not been fully studied *in vivo* and *in vitro*.

Recently, we reported that UVB-induced inflammatory responses, as well as the formation of CPD, also play an important role in the highly photo-skin carcinogenic phenotype in *Xpa* knockout mice, where the inhibition of CXCL1, a neutrophil attractant chemokine and a suggestive inflammation marker by UVB, using CXCL1 monoclonal neutralizing antibody (CXCL1-Ab), suppressed the yield of NMSC in *Xpa* knockout mice [16]. However, it remains to be clarified whether CXCL1-Ab affects the pattern of somatic

mutations in oncogenes or TSGs upon UVB exposure in the mouse skin. In this study, we analyzed NMSC of *Xpa* knockout and wild-type mice with repetitive UVB exposure using whole exome sequencing (WES) to detect distinct somatic mutation characteristics among wild-type, *Xpa* knockout, and CXCL1-Ab-administered *Xpa* knockout mice.

2 MATERIALS AND METHODS

2.1 UVB sources, mice, and skin tumor preparation

We used UVB sources installed with a bank of five TL 20W/12RS fluorescent lamps (Philips, Eindhoven, Holland) in our previous study [17]. The mice were irradiated with UVB lamps 40 cm away from the light source. We prepared *Xpa* knockout mice with CBA [12], C57BL/6, and CD-1 chimeric backgrounds backcrossed with hairless albino mice from the BALB/cA Kud-h inbred strain. All animal experiments were conducted in accordance with the guidelines for animal experimentation at Kobe University School of Medicine. Fourteen hairless wild-type mice aged 12–15 weeks were exposed to 1.8 kJ/m^2 UVB twice a week for 25 weeks. The hairless *Xpa* knockout mice were irradiated with 0.5 kJ/m^2 UVB twice a week for 10 weeks, followed by observation of skin tumor development for another 15 weeks [16]. A solution of CXCL1-Ab (R&D Systems, Minneapolis, MN) diluted to 0.5 μg/μL with phosphate-buffered saline was prepared and

administered intraperitoneally (5 μg-CXCL1-Ab/mouse) to nine hairless *Xpa* knockout mice immediately after and 24 hours after 0.5 kJ/m^2 UVB irradiation, similar to the protocol for the UVB irradiation only group (Figure 1A).

Skin tumors > 2 mm in diameter were counted. The tumors or skin were dissected under isoflurane inhalation and subjected to RNAlater stabilization solution (Thermo Fisher Scientific, Carlsbad, MA). Samples were incubated in 0.5 M ammonium thiocyanate (Wako, Osaka, Japan) in phosphate-buffered saline at room temperature for 60 min, and the epidermis of each normal-appearing skin sample was detached from the dermis [18]. The isolated epidermis or tumors were homogenized using a polytron homogenizer (KINEMATICA, Luzernerstrasse, Switzerland) and processed for DNA/RNA isolation using a QIAshredder and AllPrep DNA/RNA Micro Kit (Qiagen, Hilden, Germany). All procedures were approved by the review boards of the Institute for Experimental Animals (approval number: P191014) and the Committee on Genetically Modified Organisms (approval number:2019-R-02) of the Kobe University Graduate School of Medicine.

2.2 Whole exome sequencing

Single-nucleotide variants (SNVs) and short insertions and deletions (indels) were

identified in each pair of UVB-induced mouse skin tumors and matched skin samples that were collected from the same mouse before UVB exposure. For each sample, 200 ng of DNA was fragmented using NEBNext dsDNA Fragmentase (New England Biolabs, Ipswich, MA, USA). Sequencing libraries were constructed using the NEBNext Ultra II DNA Library Prep Kit for Illumina (New England BioLabs). Libraries were hybridized to probes of SeqCap EZ Mouse Exome Design (Roche Diagnostics, Basel, Switzerland). The quantity and size distribution of the captured libraries were assessed using a Qubit 2.0 Fluorometer (Thermo Fisher Scientific) and a Bioanalyzer 2100 (Agilent Technologies, Santa Clara, CA), respectively. The libraries were sequenced using the Illumina HiSeq 2500 platform with a 2×150-bp paired-end module (Illumina). Bioinformatic analyses for the preprocessing of the sequence data, detection of somatic mutations, and functional annotations of the identified mutations were implemented based on our previous studies [19-21] and are described in the Supplementary Materials and Methods. We explored mutational signatures characterizing the mutational processes operative in UVB-induced mouse skin tumors by fitting the spectrum of somatic single nucleotide substitutions to the Catalogue of Somatic Mutations in Cancer (COSMIC) mutation signatures [22] (see Supplementary Materials and Methods). Transcriptional strand biases of single-base substitutions and

doublet base substitutions were evaluated as described in Supplementary Materials and Methods.

2.3 Immunohistochemistry

Tumor and mouse skin specimens were collected at certain time points, fixed in 10% neutralized formalin, and embedded in paraffin. Hematoxylin and eosin staining was performed for histopathological diagnosis of the specimens. Immunohistochemical analyses using polyclonal antibodies against Trp53 protein (CM5) (Vector Laboratories, Burlingame, CA), Ras (G12D Mutant) (GeneTex, Irvine, CA), PIK3CA (Bioss, Boston, MA), and mTOR (Invitrogen, Waltham, MA) were performed according to previously described protocol [23]. All the specimens were observed and photographed using a BZ-X710 microscope (Keyence, Osaka, Japan). Ten images were randomly chosen from each sample slide, and the total area of cells positive for PIK3CA and mTOR was quantitatively evaluated using a hybrid cell count application (BZ-H4C; Keyence) in the BZ-X Analyzer software (BZ-H4A).

2.4 Statistics

The significance of the differences in skin tumor yields between groups and semi-

quantification of positive cells in immunohistochemical analysis was determined using Student's *t*-test. Statistical significance was set at $P < 0.05$.

3 RESULTS

3.1 Development of UVB-induced mice skin tumors

Xpa knockout mice have been known to have a highly photo skin carcinogenic phenotype, in which the protocol of UVB-induced skin tumors with less frequent exposure and less dose of irradiation (0.5 kJ/cm^2) would be enough for inducing skin tumors (Figure 1A). The yield of tumors in *Xpa* knockout mice was much faster than that in wild-type mice, even with small-scale irradiation (Figure 1B, C). Furthermore, we examined an additional group of developed tumors in *Xpa* knockout mice that were administered CXCL1-Ab under the exact same exposure protocol for *Xpa* knockout mice. Administration of CXCL1-Ab reduced and delayed skin tumor development compared with the UVB exposure-only group of *Xpa* knockout mice. These results are consistent with those of our previous study (Figure 1B, C) [16].

3.2 Mutational signatures of UVB-induced mice skin tumors

We performed WES for the developed tumors at 18 and 25 weeks, as well as for matched skin samples before UVB irradiation in all groups (Figure 1A). The mean average sequencing depth and coverage of ≥20 reads for the target regions were 109.0 and 95.1%, respectively. We classified the somatic SNVs into 96 mutation classes consisting of six pyrimidine substitutions (C>T, C>A, C>G, T>C, T>G, and T>A) in combination with flanking 5' and 3' bases (Figure 1D). The mutation spectrum showed that UV signature mutations, defined as C>T substitutions at dipyrimidine sites (CC, CT, and TC), accounted for the majority of the somatic SNVs in all groups, tumors of wild-type (25 weeks), *Xpa* knockout mice (18 and 25 weeks), and CXCL1-Ab administered *Xpa* knockout mice (25 weeks) (Figure 1D). Mutational signatures characterizing the mutational processes operate in each of the four groups of skin tumors, where the spectrum of somatic SNVs was fitted to the COSMIC single base substitution (SBS) signatures (https://cancer.sanger.ac.uk/signatures/sbs/) [22]. SBS2 (APOBEC family of cytidine deaminases), SBS7 (UV exposure), and SBS19 (NER-related DNA damage-induced mutation) were overrepresented in all four groups. In contrast, SBS11 (alkylating agent temozolomide as a mutagen) and SBS17a (unknown etiology) were significant, specifically in *Xpa* knockout and wild-type mice, respectively (Figure 1E).

3.3 Transcriptional strand asymmetry of somatic mutations

Somatic mutations within transcribed genome regions possibly show transcriptional strand asymmetry, reflecting transcription-associated DNA damage and transcription-coupled DNA repair [22]. We examined the transcriptional strand asymmetry of somatic mutations, including SBS (C>T) and double base substitutions (DBS) (CC>TT), between transcribed and non-transcribed strands. While somatic mutations in the tumors of wild-type mice occurred preferentially in the non-transcribed strand, *Xpa* knockout mice showed preferential mutations in the transcribed strand (Figure 1F), reflecting a deficiency in transcription-coupled nucleotide excision repair in *Xpa* knockout mice. Remarkably, somatic mutations in the tumors of *Xpa* knockout mice with CXCL1-Ab occurred preferentially in the transcribed strand, but the extent of strand bias was attenuated compared to *Xpa* knockout mice without CXCL1-Ab (Figure 1F).

3.4 Somatic mutations of oncogenes and TSGs in UVB-induced skin tumors

We sought mutations of oncogenes and TSGs that have been reported to be frequently mutated and play pivotal roles in NMCS, as well as in SCC of other organs [10,24,25]. We identified somatic mutations in several oncogenes such as *Kras*, *Hras,* and *Pik3ca*. Many mutations have been detected in TSGs, such as *Notch1*, *Trp53*, *Fat1, Nf1,* and *Smad4*.

Notably, mutations in caretaker genes such as *Fanca*, *Msh6*, *Xrcc4*, and *Xrcc5* were detected specifically in *Xpa* knockout mice (Figure 2A, S1, and Table S1).

Somatic mutations in oncogenes, such as *Kras* and *Hras*, TSGs, such as *Notch1*, *Fat2*, *Trp53*, and other key genes for developing NMSC occurred preferentially in the transcribed and non-transcribed strands in *Xpa* knockout and wild-type mice, respectively (Figure 2B). The bias toward mutations in the non-transcribed strand of *Trp53* in the tumors of wild-type mice is consistent with previous results [26,27]. Likewise, the bias of the transcribed strand of *Trp53* in the NMSC of *Xpa* knockout mice has been reported [28-31]. Moreover, G:C>T:A transversions, presumably induced by 8-oxoG, occurred predominantly in the non-transcribed strand of *Kras*, *Hras*, and *Fat1* in the tumors of *Xpa* knockout mice (Figure 2B). Amino acid substitutions of *Kras* and *Hras* were concentrated at codons 12 and 13, called hot spots, and somatic mutations of *Trp53* were localized to the DNA-binding domain. In contrast, somatic mutations in *Kmt2c*, *Kmt2d*, and *Fat1* were evenly distributed across these genes (Figure 2C) [24].

3.5 Analysis of NMSC developed with single-shot UVB irradiation

It has been experienced that tumor development can be initiated by only a single shot of UVB exposure in *Xpa* knockout mice, although it rarely occurs in wild-type hairless mice

[32]. We characterized the genomes of the tumors that developed using a single shot of UVB. After one-time irradiation with 0.5 kJ/m^2 UVB on a *Xpa* knockout mouse and the subsequent observation, half of the developed tumor was biopsied for WES and the other half was left to grow at 13 and 18 weeks. Finally, the entire tumor was excised after 25 weeks (Figure. 3A). Tumors at 13, 18, and 25 weeks were histologically diagnosed as SCC (data not shown). Furthermore, the mutation spectrum, extracted mutational signatures, and transcriptional strand asymmetry in SBS and DBS of all tumor samples across time points showed similar patterns to the tumors developed by chronic UVB exposure in *Xpa* knockout mice (Figure 3B, 3C, and 3D). Identical UV signature mutations of *Kras*, *Fat1*, and *Kmt2c* were detected at every time point. No additional mutations in cancer-related genes accumulated at later time points (Figure 3E). These results suggest that the three mutations induced by only a single shot of UVB irradiation were sufficient drivers for the initiation, promotion, and progression of NMSC in *Xpa* knockout mouse.

3.6 Effects of CXCL1-Ab on tumors in *Xpa* knockout mice

In *Xpa* knockout mice administered with CXCL1-Ab, no substitutions in *Kras* or *Hras* were observed. In contrast, a UV signature mutation of *Pik3ca* was detected (Figure. 2A,

Table S1). Although Ras/Raf/MAPK signaling was not activated by oncogenic mutations, other cell proliferation signaling pathways such as the PI3K/mTOR pathway might be activated in the tumors of CXCL1-Ab-administrated *Xpa* knockout mice. Immunohistochemical analysis also showed that PIK3CA and mTOR expression was relatively higher in the tumors of CXCL1-Ab-administered *Xpa* knockout mice than in *Xpa* knockout mice treated with UVB irradiation only (Figure 4A, 4B, and 4C).

4 DISCUSSION

In this study, we examined the genomes of *Xpa* knockout and wild-type mice. Most of the identified mutated oncogenes, such as *Hras* and *Kras*, and TSGs, such as *Apc*, *Dcc*, *Fat1*, *Kmt2c*, *Nf1*, *Notch1*, *Pten*, *Smad4*, and *Trp53,* are shared with those of other types of human cancers. Although the mutated cancer-related genes were not significantly different between *Xpa* knockout and wild-type mice, the pattern of transcriptional strand asymmetry was remarkably different, in which UV signature mutations in *Xpa* knockout and wild-type mice preferentially occurred in transcribed and non-transcribed strands, respectively. In addition, WES analysis of the exact same tumor of a *Xpa* knockout mouse with “a single shot of UVB” at different time points showed that mutations in *Kras*, *Fat1*, and *Kmt2c* with exact amino acid changes were consistently detected, suggesting that

these genes are critical for initiating steps. Together, *Kras*/*Fat1*/*Kmt2c* mutation concomitant with other oncogenes or TSGs mutating preferentially at the "transcribed strand" would be enough for the initiation as well as progression of tumors of the *Xpa* knockout genotype and be no longer indispensable for *Trp53* mutation, which is one of most critical genes for the promotion of skin tumors in wild-type mice [33].

One of the most important findings of this study is the differential transcriptional strand asymmetry of somatic mutations in *Xpa* knockout and wild-type mice. It is evident that transcription-coupled repair of exogenous DNA damage, such as UV irradiation, leads to a reduction in somatic mutations on the transcribed strand compared to the non-transcribed strand [10,27,34]. This is consistent with our results, in which C>T and CC>TT mutations were more frequent on the non-transcribed strand in tumors of wild-type mice. In sharp contrast, somatic mutations in tumors of *Xpa* knockout mice were more frequent on the transcribed strand. Although the bias of the transcribed strand in the NMSC of *Xpa* knockout mice has been reported only in *Trp*53 [28-31], this study is the first to show that the genome-wide strand bias of somatic mutations in NMSC has been identified. These transcriptional strand asymmetries were observed not only in oncogenes or TSGs but also at the genome-wide level. Since XPA repairs pyrimidine dimers with a transcribed coupled NER (TC-NER) system, the deficiency in TC-NER in *Xpa* knockout mice may

be attributed to the increased number of UV-induced mutations on the transcribed strand. At the same time, the global genome NER (GG-NER), another NER system involved in the repair of non-transcribed and transcribed strands, is also disrupted in *Xpa* knockout mice. It should be noted that cells deficient in TC-NER are more sensitive to apoptosis and prone to cell death than cells deficient in GG-NER, which is consistent with the phenotype of Cockayne syndrome, which is caused by a deficiency in TC-NER but not in GG-NER and is characterized by rarely developed skin cancers [35,36]. Our WES could not evaluate the effect of GG-NER deficiency in *Xpa* knockout mice. Whole-genome sequencing may be useful for assessing the effects of GG-NER deficiency on the patterns of somatic mutations outside of the transcribed genome regions. Further studies are required to elucidate the mechanisms by which the mutation spectrum and transcriptional strand asymmetry are shaped in the genomes of *Xpa* knockout and wild-type mice. Although XP-A is known for its severe neurodegenerative symptoms and *Xpa*-knockout mice show a much milder phenotype than humans with XP-A, most of the associated mechanisms have not been elucidated [37,38]. The analysis of somatic SNVs in the prefrontal cortex and hippocampus by single-cell whole-genome sequencing showed a significantly greater number of mutations in XP-A individuals than unaffected individuals, with ROS modification mutations specifically detected [39]. Future studies focusing on somatic

mutations and epigenetic modifications in neurons of *Xpa*-knockout mice may provide valuable clues for the elucidation of the mechanism of neurodegeneration in XP-A.

From a therapeutic perspective, the strategy targeted at mutated gene products that are involved in the initial steps of multistep skin carcinogenesis may be reasonable. Such a strategy would be effective before tumors attain intratumoral heterogeneity by acquiring additional mutations and become resistant to treatment [40]. Our data demonstrated that i) *Kras* and *Hras* were mutated in most of the *Xpa* knockout mice in a mutually exclusive manner, and ii) *KRAS* mutation was involved in the initial step of photo skin carcinogenesis, as shown by the experiment with a single UVB exposure.

An inflammatory reaction by UVB exposure in the skin plays a role in the development of skin cancers through the formation of UVB-induced 8-oxoG and subsequent neutrophil infiltration with upregulation of a number of chemokines [23], in which the yield of UVB-induced skin tumors could be suppressed by the administration of the CXCL1 antibody, a neutrophil-taxis chemokine [16]. Notably, we showed that mutations in *Kras* and *Hras* were not identified in the *Xpa* knockout group administered CXCL1-Ab. Since tumor-promoting inflammation plays a critical role in KRAS-driven carcinogenesis [41], UVB-induced inflammation and oncogenic *Kras* and *Hras* mutations are involved in skin carcinogenesis. It is possible that CXCL1-neutralizing antibody

suppresses *Kras*- and *Hras*-driven carcinogenesis by altering the immune microenvironment. Tumors in the *Xpa* knockout UVB plus CXCL1-Ab group harbored *Pik3ca* mutations instead of *Kras* and *Hras* mutations. The RAS-RAF-MEK-ERK-MAPK (RAS-MAPK) pathway can mutually and dependently or independently interact with the PI3K pathway, such as in endometrial, colon, and prostate cancer [20,42,43]. Our data showed the tendency of upregulation of some downstream proteins of PIK3CA signaling, implying that CXCL1-Ab treatment might drift from the RAS-MAPK to the PIK3CA pathway [44,45], which would have less potent effects on skin tumor production. The exact mechanism by which CXCL1-Ab affects signal transduction, including the shift from transcribed to non-transcribed prone mutation patterns, remains to be elucidated. However, this study showed that the anti-inflammatory reactions of the skin actually affect genome changes after UVB irradiation, especially the inflammatory reaction-sensitive phenotype in the xeroderma pigmentosum complementation groups. Several roles of ROS have been reported [46] and, as CXCL1 is a neutrophil migration factor, free radicals induced by neutrophils may interact with various cellular components in the tumor microenvironment and promote mutagenesis.

ACKNOWLEDGEMENTS

We thank Junko Kajiwara, Junko Kitayama, Yumiko Sato, and Keiko Nishikawa for their technical assistance.

CONFLICT OF INTEREST

The authors declare no conflicts of interest.

AUTHOR CONTRIBUTIONS

AY contributed to the data collection and wrote the initial draft of the manuscript. HN, TF, II, and CN contributed to the analysis and interpretation of the data and assisted with the preparation of the manuscript. MK designed the study, and critically reviewed the manuscript. All authors approved the final version of the manuscript and agreed to be accountable for all aspects of the work, ensuring that questions related to the accuracy or integrity of any part of the work are appropriately investigated and resolved.

DATA AVAILABILITY STATEMENT

The data supporting the findings of this study are available from the corresponding author upon reasonable request.

ORCIDs

Ai Yoshioka: https://orcid.org/0000-0001-6534-4566

Hirofumi Nakaoka: https://orcid.org/0000-0002-8454-1159

Takeshi Fukumoto: https://orcid.org/0000-0003-0364-711X

Ituro Inoue: https://orcid.org/0000-0003-1706-8493

Chikako Nishigori: https://orcid.org/0000-0002-6784-2849

Makoto Kunisada: https://orcid.org/0000-0003-2210-6108

REFERENCES

1. Kim Y, He YY. Ultraviolet radiation-induced non-melanoma skin cancer: Regulation of DNA damage repair and inflammation. Genes Dis. 2014;1(2):188-198.
2. Ikehata H, Ono T. The mechanisms of UV mutagenesis. J Radiat Res. 2011;52(2):115-125.
3. Abel EL, Angel JM, Kiguchi K, DiGiovanni J. Multi-stage chemical carcinogenesis in mouse skin: fundamentals and applications. Nat Protoc. 2009;4(9):1350-1362.
4. Yuspa SH. The pathogenesis of squamous cell cancer: lessons learned from studies of skin carcinogenesis--thirty-third G. H. A. Clowes Memorial Award Lecture. Cancer Res. 1994;54(5):1178-1189.
5. Brash DE, Rudolph JA, Simon JA, et al. A role for sunlight in skin cancer: UV-induced *p53* mutations in squamous cell carcinoma. Proc Natl Acad Sci U S A. 1991;88(22):10124-10128.
6. Pierceall WE, Goldberg LH, Tainsky MA, Mukhopadhyay T, Ananthaswamy HN. *Ras* gene mutation and amplification in human nonmelanoma skin cancers. Mol Carcinog. 1991;4(3):196-202.

7. Nishigori C, Yarosh DB, Ullrich SE, et al. Evidence that DNA damage triggers interleukin 10 cytokine production in UV-irradiated murine keratinocytes. Proc Natl Acad Sci U S A. 1996;93(19):10354-10359.
8. Nicolas M, Wolfer A, Raj K, et al. Notch1 functions as a tumor suppressor in mouse skin. Nat Genet. 2003;33(3):416-421.
9. South AP, Purdie KJ, Watt SA, et al. *NOTCH1* mutations occur early during cutaneous squamous cell carcinogenesis. J Invest Dermatol. 2014;134(10):2630-2638.
10. Martincorena I, Roshan A, Gerstung M, et al. Tumor evolution. High burden and pervasive positive selection of somatic mutations in normal human skin. Science. 2015;348(6237):880-886.
11. Bradford PT, Goldstein AM, Tamura D, et al. Cancer and neurologic degeneration in xeroderma pigmentosum: long term follow-up characterises the role of DNA repair. J Med Genet. 2011;48(3):168-176.
12. Nakane H, Takeuchi S, Yuba S, et al. High incidence of ultraviolet-B-or chemical-carcinogen-induced skin tumours in mice lacking the xeroderma pigmentosum group A gene. Nature. 1995;377(6545):165-168.
13. Sekiguchi M, Tsuzuki T. Oxidative nucleotide damage: consequences and prevention. Oncogene. 2002;21(58):8895-8904.
14. Hattori Y, Nishigori C, Tanaka T, et al. 8-hydroxy-2'-deoxyguanosine is increased in epidermal cells of hairless mice after chronic ultraviolet B exposure. J Invest Dermatol. 1996;107(5):733-737.
15. Kunisada M, Sakumi K, Tominaga Y, et al. 8-Oxoguanine formation induced by chronic UVB exposure makes *Ogg1* knockout mice susceptible to skin carcinogenesis. Cancer Res. 2005;65(14):6006-6010.
16. Kunisada M, Hosaka C, Takemori C, Nakano E, Nishigori C. CXCL1 Inhibition Regulates UVB-Induced Skin Inflammation and Tumorigenesis in *Xpa*-Deficient Mice. J Invest Dermatol. 2017;137(9):1975-1983.
17. Kunisada M, Kumimoto H, Ishizaki K, Sakumi K, Nakabeppu Y, Nishigori C. Narrow-band UVB induces more carcinogenic skin tumors than broad-band UVB through the formation of cyclobutane pyrimidine dimer. J Invest Dermatol. 2007;127(12):2865-2871.
18. Gu X, Nylander E, Coates PJ, Fahraeus R, Nylander K. Correlation between Reversal of DNA Methylation and Clinical Symptoms in Psoriatic Epidermis Following Narrow-Band UVB Phototherapy. J Invest Dermatol. 2015;135(8):2077-2083.

19. Suda K, Cruz Diaz LA, Yoshihara K, et al. Clonal lineage from normal endometrium to ovarian clear cell carcinoma through ovarian endometriosis. Cancer Sci. 2020;111(8):3000-3009.
20. Suda K, Nakaoka H, Yoshihara K, et al. Clonal Expansion and Diversification of Cancer-Associated Mutations in Endometriosis and Normal Endometrium. Cell Rep. 2018;24(7):1777-1789.
21. Yamaguchi M, Nakaoka H, Suda K, et al. Spatiotemporal dynamics of clonal selection and diversification in normal endometrial epithelium. Nat Commun. 2022;13(1):943.
22. Alexandrov LB, Kim J, Haradhvala NJ, et al. The repertoire of mutational signatures in human cancer. Nature. 2020;578(7793):94-101.
23. Kunisada M, Yogianti F, Sakumi K, Ono R, Nakabeppu Y, Nishigori C. Increased expression of versican in the inflammatory response to UVB- and reactive oxygen species-induced skin tumorigenesis. Am J Pathol. 2011;179(6):3056-3065.
24. Pickering CR, Zhou JH, Lee JJ, et al. Mutational landscape of aggressive cutaneous squamous cell carcinoma. Clin Cancer Res. 2014;20(24):6582-6592.
25. Dotto GP, Rustgi AK. Squamous Cell Cancers: A Unified Perspective on Biology and Genetics. Cancer Cell. 2016;29(5):622-637.
26. Brash DE. UV signature mutations. Photochem Photobiol. 2015;91(1):15-26.
27. Yogianti F, Kunisada M, Ono R, Sakumi K, Nakabeppu Y, Nishigori C. Skin tumours induced by narrowband UVB have higher frequency of *p53* mutations than tumours induced by broadband UVB independent of *Ogg1* genotype. Mutagenesis. 2012;27(6):637-643.
28. Takeuchi S, Nakatsu Y, Nakane H, et al. Strand specificity and absence of hot spots for *p53* mutations in ultraviolet B-induced skin tumors of *XPA*-deficient mice. Cancer Res. 1998;58(4):641-646.
29. Tanaka K, Kamiuchi S, Ren Y, et al. UV-induced skin carcinogenesis in xeroderma pigmentosum group A (XPA) gene-knockout mice with nucleotide excision repair-deficiency. Mutat Res. 2001;477(1-2):31-40.
30. de Vries A, Berg RJ, Wijnhoven S, et al. XPA-deficiency in hairless mice causes a shift in skin tumor types and mutational target genes after exposure to low doses of U.V.B. Oncogene. 1998;16(17):2205-2212.
31. Kucab JE, van Steeg H, Luijten M, et al. *TP53* mutations induced by BPDE in Xpa-WT and Xpa-Null human *TP53* knock-in (Hupki) mouse embryo fibroblasts. Mutat Res. 2015;773:48-62.
32. Hsu J, Forbes PD, Harber LC, Lakow E. Induction of skin tumors in hairless mice

by a single exposure to UV radiation. Photochem Photobiol. 1975;21(3):185-188.
33. Ziegler A, Jonason AS, Leffell DJ, et al. Sunburn and p53 in the onset of skin cancer. Nature. 1994;372(6508):773-776.
34. Alexandrov LB, Nik-Zainal S, Wedge DC, Campbell PJ, Stratton MR. Deciphering signatures of mutational processes operative in human cancer. Cell Rep. 2013;3(1):246-259.
35. Hanawalt PC. Subpathways of nucleotide excision repair and their regulation. Oncogene. 2002;21(58):8949-8956.
36. Ren Y, Saijo M, Nakatsu Y, Nakai H, Yamaizumi M, Tanaka K. Three novel mutations responsible for Cockayne syndrome group A. Genes Genet Syst. 2003;78(1):93-102.
37. Shinomiya H, Yamashita D, Fujita T, et al. Hearing Dysfunction in *Xpa*-Deficient Mice. Front Aging Neurosci. 2017;9:19.
38. Nishigori C, Nakano E, Masaki T, et al. Characteristics of Xeroderma Pigmentosum in Japan: Lessons From Two Clinical Surveys and Measures for Patient Care. Photochem Photobiol. 2019;95(1):140-153.
39. Lodato MA, Rodin RE, Bohrson CL, et al. Aging and neurodegeneration are associated with increased mutations in single human neurons. Science. 2018;359(6375):555-559.
40. McGranahan N, Swanton C. Clonal Heterogeneity and Tumor Evolution: Past, Present, and the Future. Cell. 2017;168(4):613-628.
41. Kitajima S, Thummalapalli R, Barbie DA. Inflammation as a driver and vulnerability of KRAS mediated oncogenesis. Semin Cell Dev Biol. 2016;58:127-135.
42. Yuan TL, Cantley LC. PI3K pathway alterations in cancer: variations on a theme. Oncogene. 2008;27(41):5497-5510.
43. Carracedo A, Ma L, Teruya-Feldstein J, et al. Inhibition of mTORC1 leads to MAPK pathway activation through a PI3K-dependent feedback loop in human cancer. J Clin Invest. 2008;118(9):3065-3074.
44. McCubrey JA, Steelman LS, Chappell WH, et al. Roles of the Raf/MEK/ERK pathway in cell growth, malignant transformation and drug resistance. Biochim Biophys Acta. 2007;1773(8):1263-1284.
45. Castellano E, Downward J. RAS Interaction with PI3K: More Than Just Another Effector Pathway. Genes Cancer. 2011;2(3):261-274.
46. Ferguson LR. Chronic inflammation and mutagenesis. Mutat Res. 2010;690(1-2):3-11.

SUPPORTING INFORMATION

The supplementary data associated with this article can be found in the online version of the article on the publisher's website.

Supplementary Figure. S1

Supplementary Table S1

Supplementary Materials and Methods

FIGURE LEGENDS

FIGURE 1. UVB irradiation induced skin tumors' formation and mutation burden in *Xpa* knockout mice

(A) A study design of UVB irradiation and sample collection for skin and skin tumors. The wild-type mice (n=14) have been irradiated at 1.8 kJ/m^2 UVB for 25 weeks, whereas *Xpa* knockout mice (n=16) have been irradiated at 0.5 kJ/m^2 UVB for 10 weeks, followed by the observation for 15 weeks and the same for *Xpa* knockout mice (n=9) administrated with CXCL1-Ab. The numbers (N) correspond to the number of each tumor sample

analyzed by whole exome sequencing (WES). Arrowheads indicate the time points of collections of normal-appearing skin for histological evaluation. (B) The average number of skin tumors are shown. The statistical difference between the average number of skin tumors of *Xpa* knockout mice and CXCL1-Ab-administered *Xpa* knockout mice at 25 weeks was indicated. Error bars represent mean ±SD. (C) The tumor induction rate (%) in wild-type, *Xpa* knockout, and CXCL1-Ab-administered *Xpa* knockout mice are shown. (D) The mutation spectrum of each group of mice with whole genome sequencing analysis. The proportion of somatic SNVs of single base substitutions (SBSs); C>A, C>G, C>T, T>A, T>C, T>G along with the adjacent 5' and 3' bases are shown, e.g. C>A has 16-pattern corresponding adjacent bases (gray lined order). (E) Bar chart representing the results of the Bayesian inference by using sigfit to determine the contribution of the COSMIC mutational signatures to somatic SNVs. The lower and upper limits of the 90% highest posterior density interval for each signature exposure are shown. (F) The strand bias (transcribed strand, blue bar; non-transcribed strand, red bar) of mutation along with dinucleotide base substitutions (DBSs) featuring UV signature mutation corresponding mutation spectrum of each group of mice are shown.

FIGURE 2. Overview of somatic mutated oncogenes and tumor suppressor genes in

UVB-induced skin tumors

(A) Summary of mutant allele frequency (MAF) for each mutated oncogenes and tumor suppressor genes listed in Table S1. The color differentiates the type of mutation: missense, nonsense and others. The density of color indicates the MAF in each gene and are divided into colored column if there are more than two mutations in the same gene. The asterisk indicates the mutation at dinucleotides base substitutions. (B) The tendency of gene mutation in the transcribed or non-transcribed strand of each oncogene and tumor suppressor genes are shown as (A). The UV signature mutation composed of C>T substitutions at dipyrimidine sites (CC, CT, and TC) are represented in the T strand as a yellow box and the NT strand as an orange box, respectively. The reactive oxygen species (ROS) modification mutations are G>T substitutions represented with a green (transcribed strand) and a light gray box (non-transcribed strand), respectively. Other base substitution patterns are shown in a purple box. The asterisk indicates the mutation at dinucleotides base substitutions. (C) The loci of amino acid changes in the domain of some extracted protein structure. Each circle, triangle, and square indicates UV signature mutations depending on the mutated transcribed or non-transcribed strand and non-UV signature mutations, respectively, and the colors of the symbols correspond to each sample group.

FIGURE 3. Analysis of skin tumor developed with one-time UVB irradiation

(A) A study design of UVB irradiation and sample collection of skin tumors of a *Xpa* knockout mouse (n=1), exposed to single 0.5 kJ/m^2 UVB irradiation followed by observation for 25 weeks. In 13, 18 and 25 weeks, half of the tumors are biopsied for WES and the other half are left to grow and for observation. (B) The mutation spectrum of three tumors consisting of all time points. (C) Bar chart representing the results of the Bayesian inference using sigfit to determine the contribution of the COSMIC mutational signatures to somatic SNVs. The lower and upper limits of the 90% highest posterior density interval for each signature exposure are shown. (D) The strand bias (transcribed strand, blue bar; non-transcribed strand, red bar) of mutation along with dinucleotide base substitutions corresponding to the mutation spectrum of the three tumor samples are shown. (E) Detection of filtered mutated genes in developed skin tumors at all time points. The mutant allele frequencies (MAFs) of *Kras*, *Fat1*, and *Kmt2c* at each time point are shown. The color differentiates the type of mutation: missense and nonsense. The density of color indicates the MAF each gene with details on amino acid change, base substitution, adjacent sequences, and strand of UV signature mutation are shown.

FIFURE 4. Histological analysis of UVB-induced skin tumors treated with CXCL1 antibody in *Xpa* knockout mice

(A) Immunohistochemical analysis using polyclonal antibodies against PIK3CA and mTOR along with hematoxylin and eosin (H&E) staining was performed on tumor samples from *Xpa* knockout and *Xpa* knockout plus CXCL1-Ab mice. Number # represents the mouse ID. Scale bar = 100 μm. Each inset photograph shows the positive features of each section. (B, C) Semi-quantification of tumor cells positive for PIK3CA and mTOR polyclonal antibodies by computing the cell counts. Statistically significant differences between the *Xpa* knockout and *Xpa* knockout plus CXCL1-Ab groups are shown. $*P < 0.05$; $**P < 0.01$. Error bars represent mean ±SD.

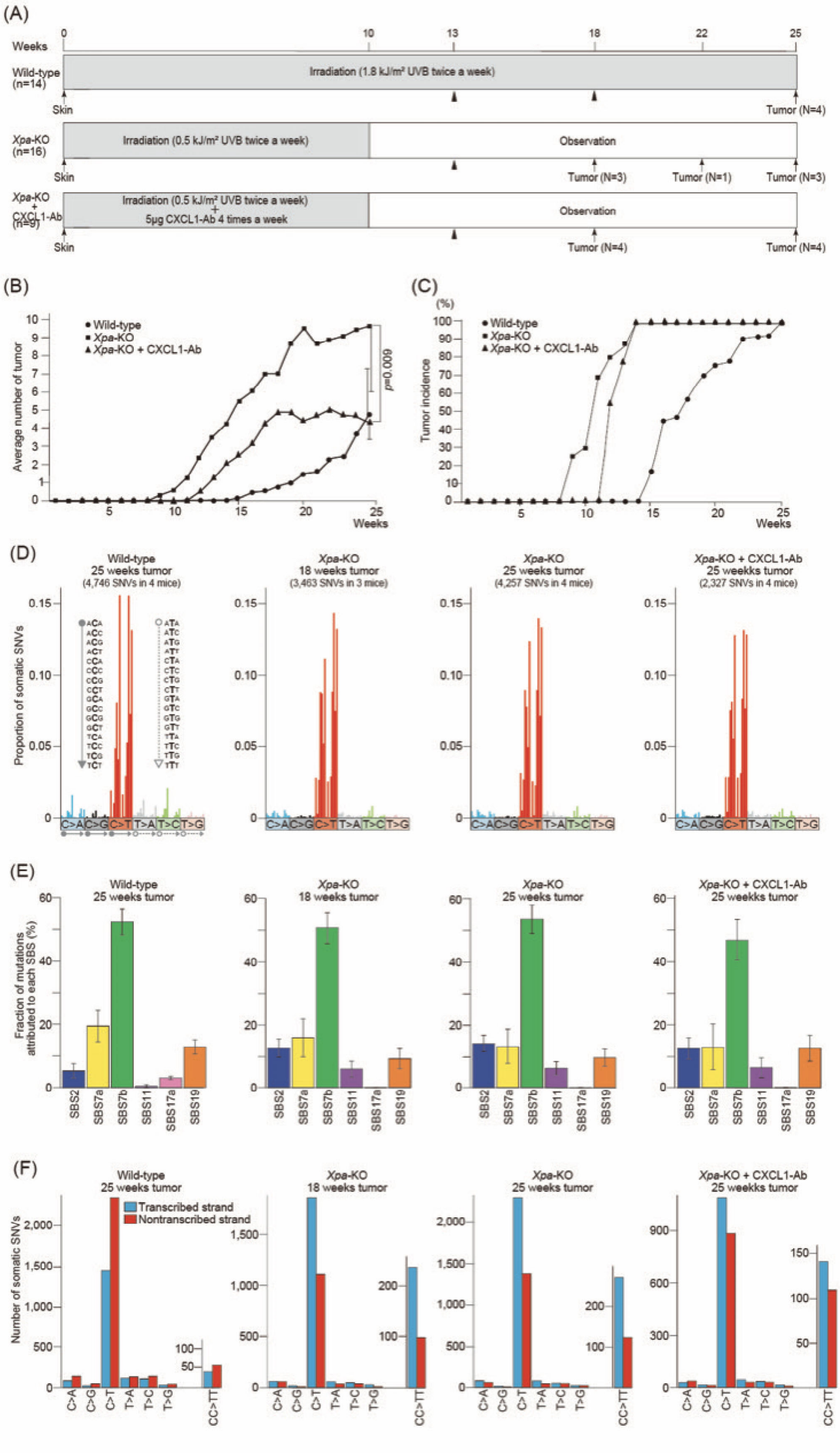
(A)
Weeks
0
10
13
18
22
25
Wild-type (n=14)
Irradiation (1.8 kJ/m² UVB twice a week)
Skin
Tumor (N=4)
Xpa-KO (n=16)
Irradiation (0.5 kJ/m² UVB twice a week)
Observation
Skin
Tumor (N=3)
Tumor (N=1)
Tumor (N=3)
Xpa-KO + CXCL1-Ab (n=9)
Irradiation (0.5 kJ/m² UVB twice a week)
+
5μg CXCL1-Ab 4 times a week
Observation
Skin
Tumor (N=4)
Tumor (N=4)
(B)
Wild-type
Xpa-KO
Xpa-KO + CXCL1-Ab
Average number of tumor
p=0.009
Weeks
(C)
(%)
Wild-type
Xpa-KO
Xpa-KO + CXCL1-Ab
Tumor incidence
Weeks
(D)
Wild-type
25 weeks tumor
(4,746 SNVs in 4 mice)
Xpa-KO
18 weeks tumor
(3,463 SNVs in 3 mice)
Xpa-KO
25 weeks tumor
(4,257 SNVs in 4 mice)
Xpa-KO + CXCL1-Ab
25 weekks tumor
(2,327 SNVs in 4 mice)
Proportion of somatic SNVs
C>A C>G C>T T>A T>C T>G
(E)
Wild-type
25 weeks tumor
Xpa-KO
18 weeks tumor
Xpa-KO
25 weeks tumor
Xpa-KO + CXCL1-Ab
25 weekks tumor
Fraction of mutations attributed to each SBS (%)
SBS2
SBS7a
SBS7b
SBS11
SBS17a
SBS19
(F)
Wild-type
25 weeks tumor
Xpa-KO
18 weeks tumor
Xpa-KO
25 weeks tumor
Xpa-KO + CXCL1-Ab
25 weekks tumor
Transcribed strand
Nontranscribed strand
Number of somatic SNVs
C>A
C>G
C>T
T>A
T>C
T>G
CC>TT

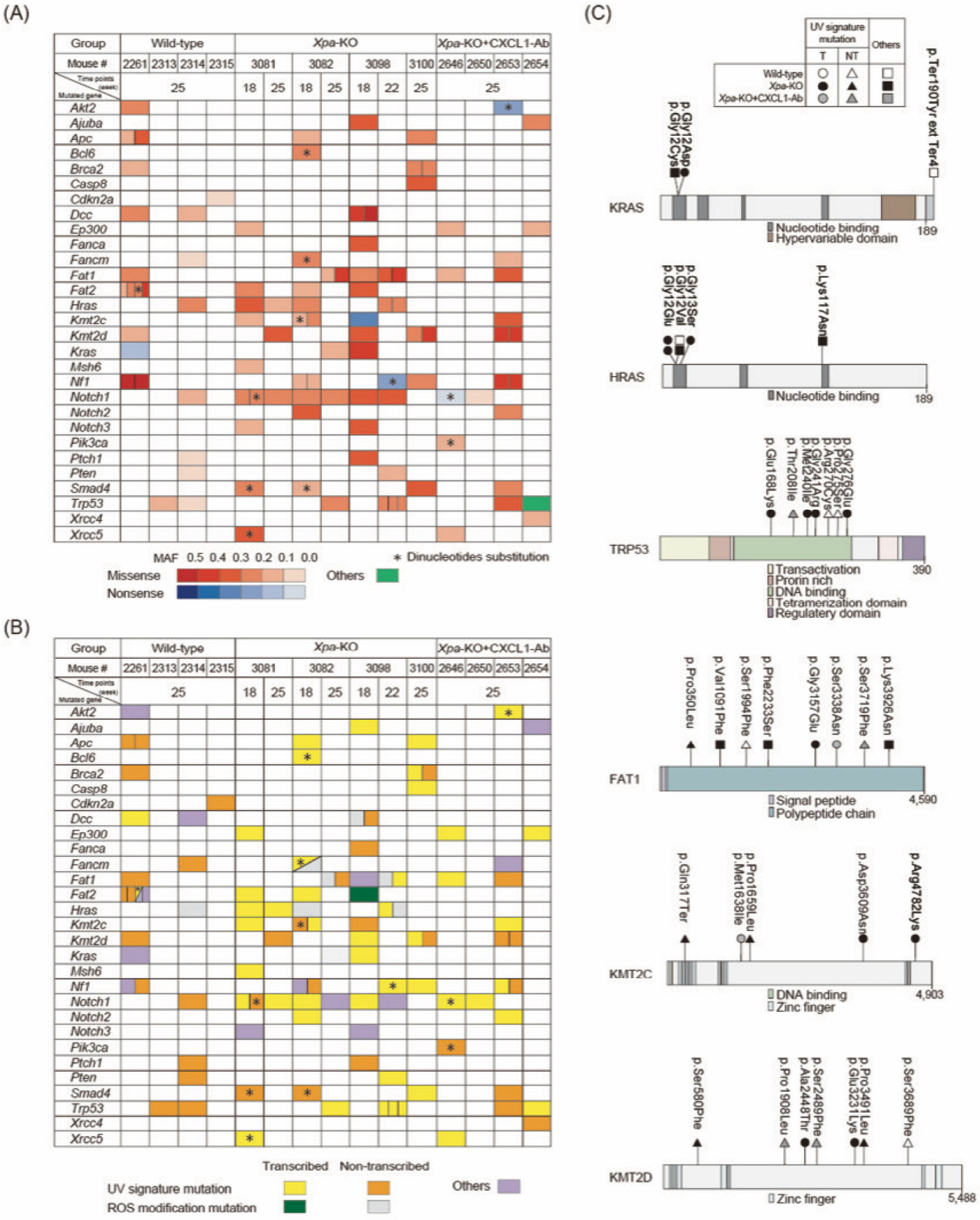
(A)
Group
Wild-type
Xpa-KO
Xpa-KO+CXCL1-Ab
Mouse #
2261 2313 2314 2315 3081 3082 3098 3100 2646 2650 2653 2654
Time points (week)
Mutated gene
25 18 25 18 25 18 22 25 25
Akt2
Ajuba
Apc
Bcl6
Brca2
Casp8
Cdkn2a
Dcc
Ep300
Fanca
Fancm
Fat1
Fat2
Hras
Kmt2c
Kmt2d
Kras
Msh6
Nf1
Notch1
Notch2
Notch3
Pik3ca
Ptch1
Pten
Smad4
Trp53
Xrcc4
Xrcc5
MAF 0.5 0.4 0.3 0.2 0.1 0.0
* Dinucleotides substitution
Missense
Nonsense
Others
(B)
Group
Wild-type
Xpa-KO
Xpa-KO+CXCL1-Ab
Mouse #
2261 2313 2314 2315 3081 3082 3098 3100 2646 2650 2653 2654
Time points (week)
Mutated gene
25 18 25 18 25 18 22 25 25
Akt2
Ajuba
Apc
Bcl6
Brca2
Casp8
Cdkn2a
Dcc
Ep300
Fanca
Fancm
Fat1
Fat2
Hras
Kmt2c
Kmt2d
Kras
Msh6
Nf1
Notch1
Notch2
Notch3
Pik3ca
Ptch1
Pten
Smad4
Trp53
Xrcc4
Xrcc5
Transcribed
Non-transcribed
UV signature mutation
ROS modification mutation
Others
(C)
UV signature mutation
T
NT
Others
Wild-type
Xpa-KO
Xpa-KO+CXCL1-Ab
p.Gly12Asp
p.Gly12Cys
p.Ter190Tyr ext Ter4
KRAS
Nucleotide binding
Hypervariable domain
189
p.Gly13Ser
p.Gly12Val
p.Gly12Glu
p.Lys117Asn
HRAS
Nucleotide binding
189
p.Glu168Lys
p.Thr208Ile
p.Met240Ile
p.Gly241Arg
p.Arg270Cys
p.Pro278Ser
p.Gly279Glu
TRP53
Transactivation
Prorin rich
DNA binding
Tetramerization domain
Regulatery domain
390
p.Pro350Leu
p.Val1091Phe
p.Ser1994Phe
p.Phe2233Ser
p.Gly3157Glu
p.Ser3338Asn
p.Ser3719Phe
p.Lys3926Asn
FAT1
Signal peptide
Polypeptide chain
4,590
p.Gln317Ter
p.Pro1659Leu
p.Met1638Ile
p.Asp3609Asn
p.Arg4782Lys
KMT2C
DNA binding
Zinc finger
4,903
p.Ser580Phe
p.Pro1908Leu
p.Ala2448Thr
p.Ser2489Phe
p.Pro3491Leu
p.Glu3231Lys
p.Ser3689Phe
KMT2D
Zinc finger
5,488

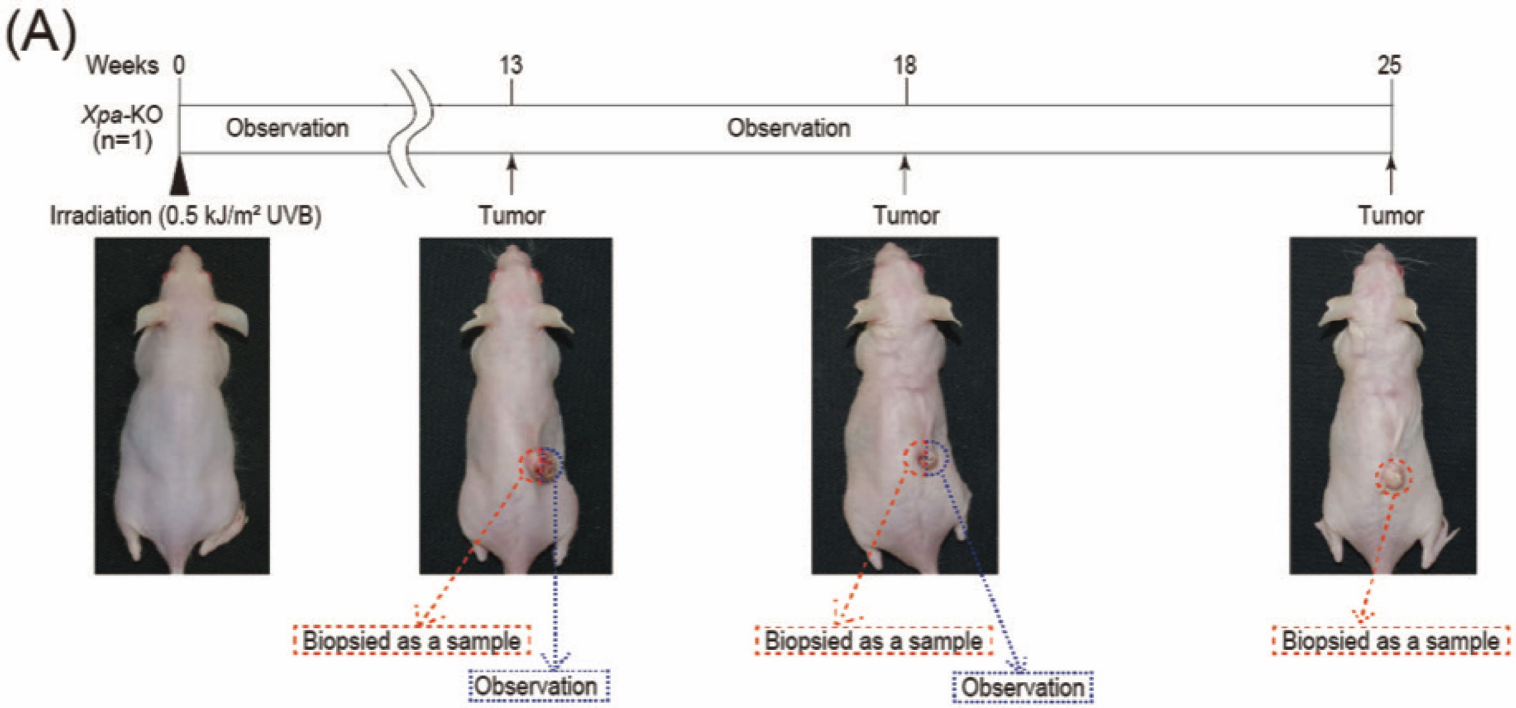

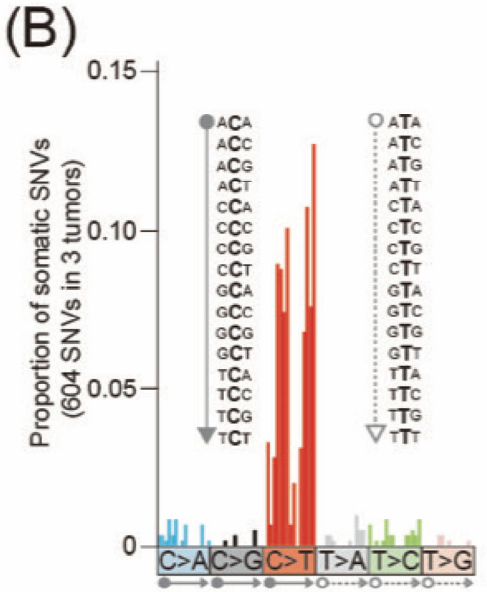

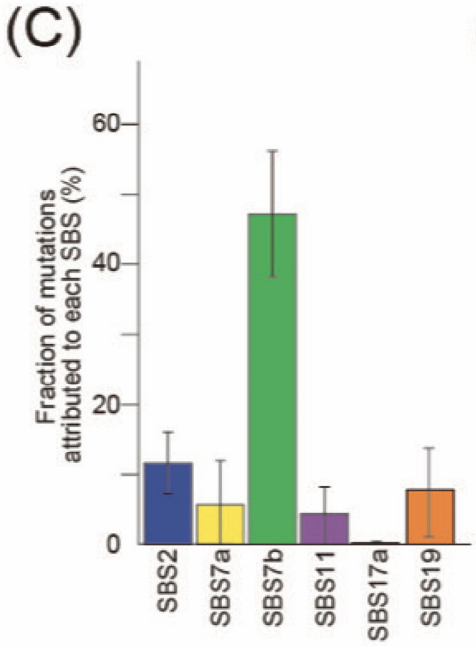

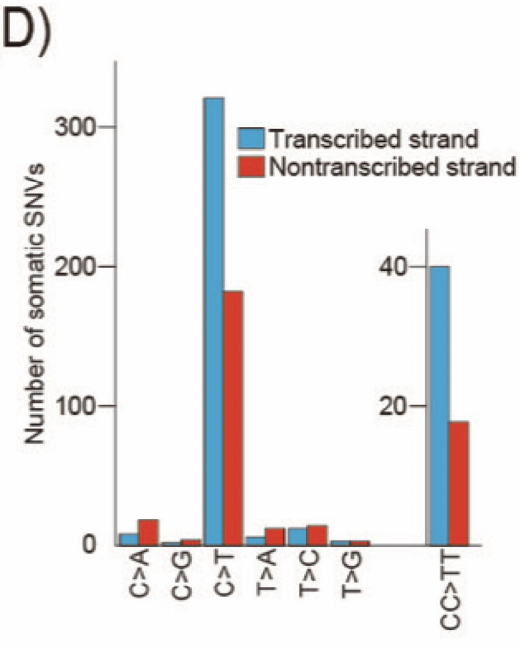

(E)

Mutated gene	MAF in tumors Time points (weeks)			Amino acid change	Base substitution	Sequence	UV signature mutation strand (C>T)
	13	18	25				
Kras				p.Gly12Asn	GG>AA	gct GGt ggc	T
Fat1				p.His3543Tyr	C>T	atc Cac cc	NT
Kmt2c				p.Trp1050Ter	GG>AA	gtt tGG tgc	T

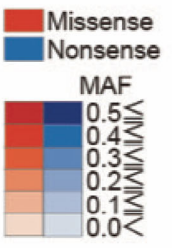

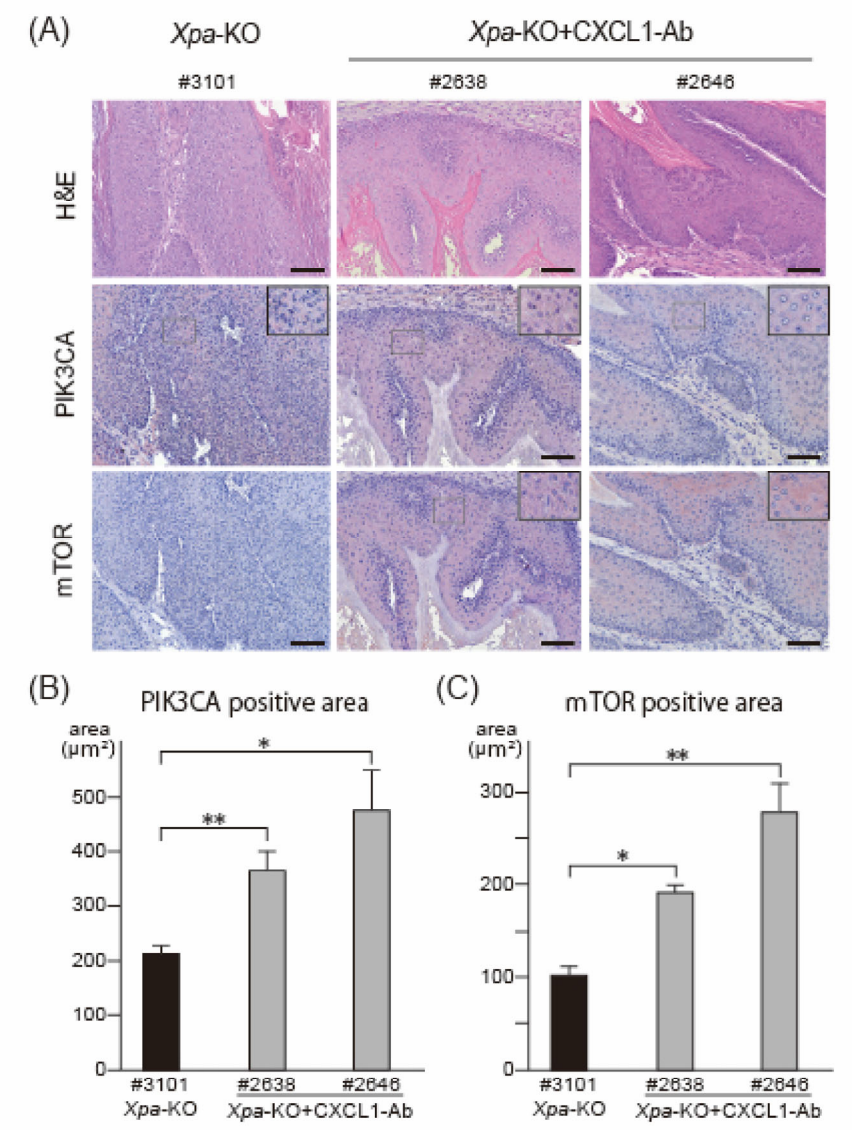
(A)
Xpa-KO
Xpa-KO+CXCL1-Ab
#3101
#2638
#2646
H&E
PIK3CA
mTOR
(B)
PIK3CA positive area
area (μm²)
500
400
300
200
100
0
*
**
#3101 Xpa-KO
#2638
#2646
Xpa-KO+CXCL1-Ab
(C)
mTOR positive area
area (μm²)
300
200
100
0
**
*
#3101 Xpa-KO
#2638
#2646
Xpa-KO+CXCL1-Ab